Machine-Learning-Based Functional Microcirculation Analysis

Ossama Mahmoud[1], GH Janssen[2,3], Mahmoud R. El-Sakka[1]

[1] Department of Computer Sciences, Western University, London (ON), Canada
[2] Department of Medical Biophysics, Western University, London (ON), Canada
[3] Centre for Critical Illness Research, Lawson Health Research Institute, London (ON), Canada

Abstract

Analysis of microcirculation is an important clinical and research task. Functional analysis of the microcirculation allows researchers to understand how blood flowing in a tissues' smallest vessels affects disease progression, organ function, and overall health. Current methods of manual analysis of microcirculation are tedious and time-consuming, limiting the quick turnover of results. There has been limited research on automating functional analysis of microcirculation. As such, in this paper, we propose a two-step machine-learning-based algorithm to functionally assess microcirculation videos. The first step uses a modified vessel segmentation algorithm to extract the location of vessel-like structures. While the second step uses a 3D-CNN to assess whether the vessel-like structures contained flowing blood. To our knowledge, this is the first application of machine learning for functional analysis of microcirculation. We use real-world labelled microcirculation videos to train and test our algorithm and assess its performance. More precisely, we demonstrate that our two-step algorithm can efficiently analyze real data with high accuracy (90%).

Introduction

For many years, researchers have used the integrity of microcirculation to understand disease progression and overall health (Tafner et al. 2017). The microcirculation consists of the tissue's smallest vessels, ranging from only 5 to 100 micrometers in diameter. These microvessels include capillaries, arterioles, and venules (Tafner et al. 2017).
While larger microvessels can accommodate a robust flow of blood, to maximize oxygen off-loading in the tissue, capillary blood flow consists of a single file of red blood cells, interspaced with plasma gaps.

To examine the microvasculature, both the structure of the vascular network and the blood flow in functionally perfused microvessels, need to be assessed via *intravital video microscopy* (IVM).

The functionality of these microvessels, i.e., the ability to carry blood flow, has significant implications for organ function during disease progression and overall health. As such, IVM is used in various medical domains to examine the microcirculation and to understand disease processes and their effects on the microcirculation (Ellis 2005; Lawendy 2016; Yeh 2017).

The quality of a tissue's microcirculation can be measured through its vascular density. Usually, vascular density for a region of tissue is determined by taking the total number of flowing microvessels across a cross-section divided by the surface area of the region examined (Charlton 2017).

Calculating vascular density proves to be a time-consuming and tedious task in practice, as it requires the visual assessment of hundreds of vessels across many frames in a microcirculation video.

Although the improvement in the speed of acquisition and quality of microscopic videos, the analysis of the experimental video data is still made by visual inspection. This time-consuming task prevents efficient use of microcirculation analysis in research. Moreover, to ensure the quality of the analysis, visual analysis is often repeated by two or more independent analyzers, compounding this problem even further. The time-intensive nature of the manual analysis is mainly due to the complexity of the video images involved, often containing a large number of similar stagnant or dynamically moving structures (i.e., red blood cells), as well as sudden changes in contrast or movement artifacts of the tissue.

Although many algorithms have been developed for analyzing the structural component of microcirculation, the functionality of microvascular blood flow is a critical parameter for assessing the development of microvascular dysfunction. As of today, to the best of our knowledge, this is the first application of machine learning for the simultaneously assessment of both vessel structure and vessel blood flow functionality

In this paper, we present a two-step machine-learning-based algorithm for the functional and structural analysis

of microcirculation. The first step of the algorithm uses the well-established Steger Unbiased Detector of Curvilinear Structures to segment the vessel structures. While the second uses a trained *3D Convoluted Neural Network* (3D-CNN) to determine whether a vessel is flowing or not.

Related work

Vessel segmentation algorithms are commonly used to analyze the structural component of the microcirculation network. As such, many algorithms exist to segment vessel structures. The most preliminary and basic is the Steger Unbiased Detector of Curvilinear Structures, which relies on measuring gradients across the image and modelling the mathematical structure of a curved vessel (Steger 1998). Although the algorithm has gone through several improvements over the years (Bezemer et al. 2011; Dimir et al. 2012; Jiang, Bainbridge-Smith, Morris 2007), it is still considered a robust vessel segmentation algorithm. (Dimir et al. 2012)

As the focus of this paper is the functional analysis of microcirculation, we focus less on segmentation, and more on flow assessment. Currently, there exist two proposed algorithms for the functional analysis of microcirculation flow. Bezemer et al. (2011) developed an algorithm for detecting perfusion of the blood vessels called *Temporal* Side-stream-dark-field *Image Contrast Analysis* (tSICA). The tSICA algorithm utilizes the changes in the intensity of flowing blood to identify whether blood was flowing through a vessel or not. Liu et al. (2015) developed an algorithm for measuring the velocity of microcirculation blood flow from videos of microcirculation. This algorithm relied on projecting vessel in one direction using a technique called Epipolar-Plane Image analysis. However, both algorithms showed limited generalizability to faster-moving blood vessels. To our knowledge, there has been no machine-learning-based approach to the functional analysis of microcirculation.

Methods

Data

The dataset used for training the machine learning algorithm was acquired through the manual analysis of IVM videos, using the method described by DeBacker in 2007. To sample the flowing/non-flowing vessels in each video, various equidistant horizontal and vertical lines are superimposed on the microcirculation video, then all flowing and non-flowing vessels intersecting these equidistance lines are digitally recorded.

The final dataset contained 32,213 labelled vessels generated from 458 IVM videos, as well as a held-out set of 34 unlabeled IVM videos. As vessels from the same IVM video appear very similar to each other, the dataset was split into two groups based on videos and not individual vessel examples. This resulted in a training set of 392 labelled IVM videos used to train and validate the CNN and a separate test set containing 66 IVM videos used to test the algorithm's performance. Datapoints from either set were only used in the training or test dataset.

Preprocessing

All captured videos underwent a preprocessing step to ensure they can be processed by the two-step algorithm

As the microcirculation videos are captured in living tissue, they are prone to unintended motion. As such, all videos are first stabilized using traditional block matching algorithms like the one used by Demir et al. (2009). The algorithm estimates the motion between the first frame of the video and all subsequent frames then removes any

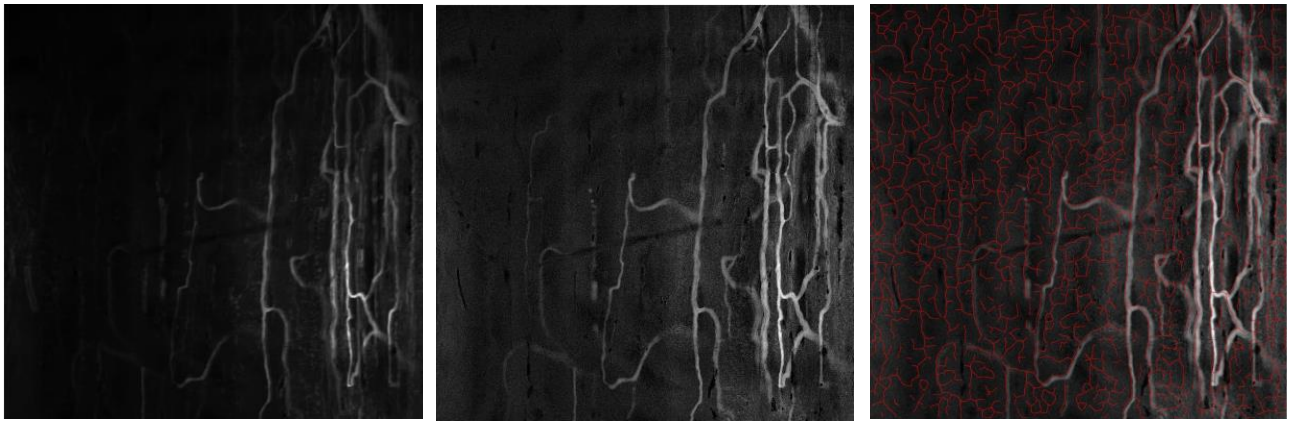

(a) (b) (c)

Figure 1: (a) SAD image of a FOV (400 × 400 µm) in the EDL muscle of a rat; clearly visible are the highlighted structures associated with the vasculature, (b) SAD image after CLAHE and Video Stabilization is applied, (c) results of Steger Curvilinear Detector (red) superimposed on SAD image.

frames with a horizontal or vertical velocity greater than 0.3 pixels per second from the sequence of microcirculation images.

Following video stabilization, a single *sum of absolute differences* (SAD) image is used to summarize the microcirculation video in one image. Creating the SAD image helps increase the speed of manual analysis as only areas with significant motion are visible in the SAD image, thus including actively flowing vessels (Japee 2005). To create this image, the frame to frame difference in pixel intensity is calculated for every pixel, and the absolute value is summed up. This results in a 2D image representation of the microcirculation video, as seen in Figure 1(a).

This SAD image is further processed by applying a *Contrast Limited Adaptive Histogram Equalization* (CLAHE) to the SAD images to enhance the contrast between the highlighted vessel structures and the background (Demir 2012), the difference, in contrast, is evident when comparing Figure 1(a) and Figure 1(b)**.**

Our Two-step Algorithm

The two-step algorithm for functional microcirculation analysis consists of two separate steps. The first step identifies the location and outline of the vessels in the previously created SAD image (i.e., vessel segmentation), while the second step involves determining whether these identified vessel structures are actively perfused with flowing blood.

First Step: Vessel Segmentation

The goal of the first step is to locate all vessel structures. The SAD image previously created in the preprocessing step acts as input to the first step of the two-step algorithm. Using the Unbiased Detector of Curvilinear Structures developed by Steger, all vessel-like structures are identified by examining the degree and direction of intensity changes in the image (Steger 1998); the resulting vessel-like structures comprise of both flowing vessels and non-flowing artifacts.

To further improve the Steger's Curvilinear Detector, we included two additional modifying steps to the vessel segmentation algorithm. First, any discontinuities in the initial superimposed vessel segmentation are filled using a morphological close operator applied to a binary vessel skeleton (A. Jain 1986). Second, all vessels that are shorter than 4 pixels are removed; Figure 1(c) shows the results of the modified Steger Curvilinear Detector superimposed on the SAD image. The vessels identified by the modified Sager Curvilinear detector are then intersected with various cross-sectional vertical and horizontal lines and only vessels intersecting these lines are sent to the next step of the algorithm.

Second Step: Determining Blood Flow

The second step seeks to identify whether a cross-section of a vessel structure belongs to a flowing vessel or a non-flowing vessel.

For every pixel in a vessel's cross-section, a surrounding area of 16×16 pixels is defined for 200 consecutive frames, thus creating a 16×16×200 data block with 65,536 data points. An area of 16×16 was chosen by microcirculation expert consultation. A 16×16 area would be sufficient in observing enough of the vessel to identify the flow. Two hundred frames were used to ensure enough time had passed for slower blood flow to appear.

Each data block is the input for the proposed spatial-temporal 3D-CNN (Ji et al. 2013). As the 3D-CNN is applied to every pixel in a vessel's cross-section, a percentage of greater than 50% of cross-sectional pixels predicted as flowing is used as a threshold to classify the vessel as flowing or not. An example of this is shown in Figure 2, where 75% of the pixels in the cross-section of the vessel are predicted to be (3 pixels) flowing while one pixel is to be not flowing. As the percent of flowing pixels is greater than the 50% threshold, we predict this vessel as flowing.

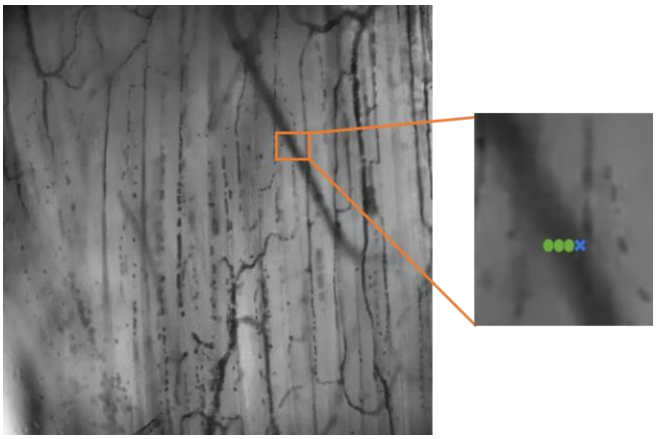

Figure 2. Each pixel in a detected vessel's cross-section is sent into the CNN, and a binary value is returned indicating if it is flowing, green circle, or not, a blue "x". The percentage of flowing pixels is then used to determine if the vessel is flowing or not.

3D-CNN architecture

The full architecture of the 3D-CNN is shown in Figure 3. As the input data has a third dimension (i.e., time), the convolutional layer and the pooling layer of the network consist of three-dimensional kernels. The 3D-CNN consists of two hidden 3D convolution layers, one with eight 7×7×7 convolution filters, and the other with eight 5×5×5 convo-

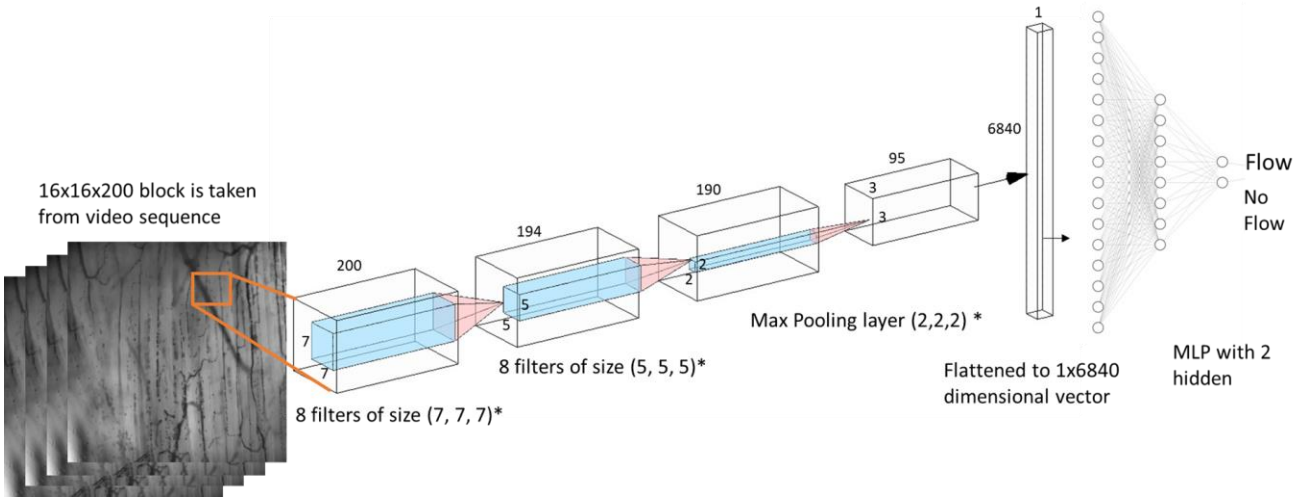

Figure 3: 3D-CNN Architecture showing input of 16×16×200 data block, and final binary output, indicating flowing or not. *Showing one out of 8 filters

lution filters. The convolution filters are followed by a max-pooling layer of 8 filters of size 2×2×2. The max-pooling layers work to reduce the representation of the output of the convolution layers. The output of the max-pooling layer is then flattened to a vector of size 6840×1, which is then fed into a traditional *Multi-layer perception* (MLP) with two hidden layers of size 16 and 8. The weights in the MLP are learned and binary output is generated, indicating whether the input pixel is of a flowing vessel or not. This architecture was chosen through validation on the validation set. Models with smaller sized filters and less hidden layers did not capture enough of the data to draw conclusions, on larger vessels. However, a deeper network with more filters, did little to change the performance of the models and as such, were not used. Training of the CNN was done over 100 epochs on a batch size of 30.

Results

3D-CNN Results

To test the 3D-CNN, a test set of 4,404 never seen before examples vessels were labelled as flowing or not. Table 1 and Table 2 summarize the performance of the CNN network on the test set. The model performs exceptionally well, with an accuracy of 90%.

The positive predictive value is 0.93, which means, on average, when the 3D-CNN predicts a flowing vessel to be flowing, it will be right 93% of the time. On the other hand, the negative predicted value is 0.81. Therefore, when the CNN network predicts a vessel to be non-flowing, there is an 81% chance it will be correct.

Table 1. Normalized confusion matrix showing results of 3D-CNN on the test set

	Predicted not flowing	Predicted flowing
True not flowing	0.77	0.23
True flowing	0.05	0.95

End-to-End Real-World Testing

To test the performance of the entire algorithm, the complete two-step algorithm was applied to 34 non-labelled microcirculation videos. The algorithm was applied after completion of the experiments and data collection mimicking a real-world application. The result was then reviewed and verified by an expert labeler, to compare performance in a real-world deployment of the algorithm.

Table 2. Evaluation metrics of 3D-CNN in percent for test set

Evaluation Metrics	Accuracy	Precision	Sensitivity	f1-score	Negative predicted value
Percentage	0.90	0.93	0.95	0.94	0.81

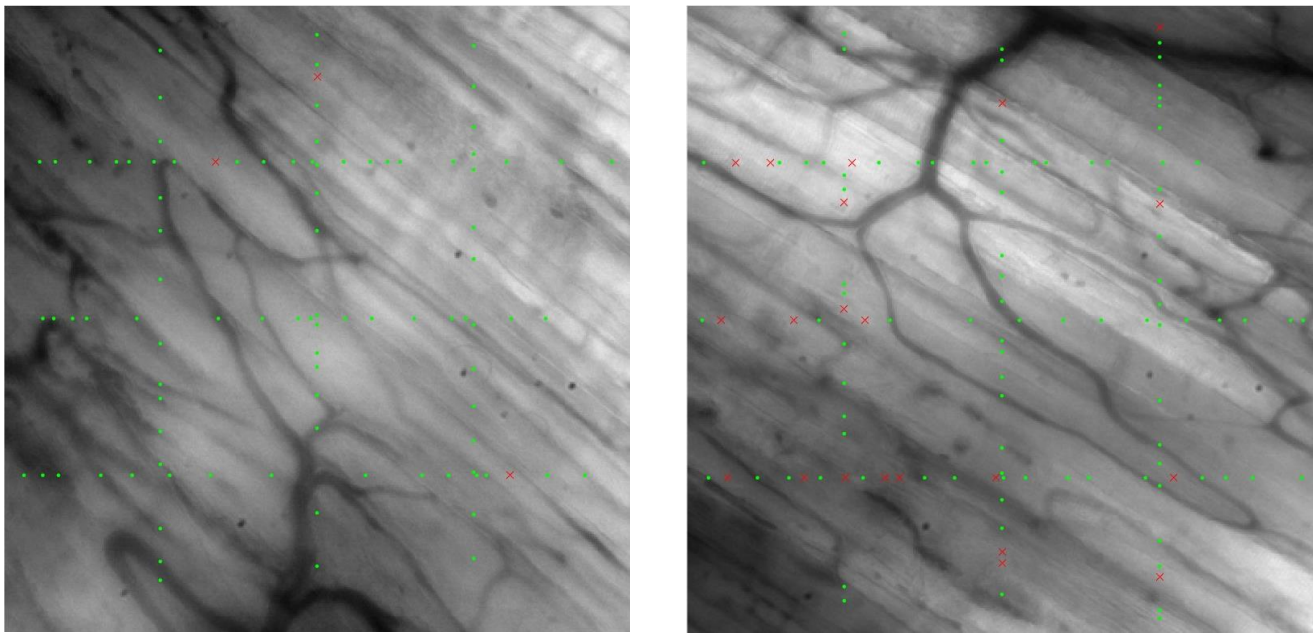

Figure 4. Final End-to-End two-step algorithm results overlaid on frame from microcirculation video. A green circle indicates a perfused microvessel, a red "x" indicates a non-perfused artifact, discovered by the step 1, but then reject in step 2 by the 3D-CNN

The percentage of incorrect points detected per an experiment as well as the percent of missed points observed by the reviewer and not the algorithm is used as a performance metric. Some of the visual results of this analysis are seen in Figure 4.

The algorithm captures about 83% of all vessels, with an error rate of only 3.5%. This demonstrates that although the algorithm has difficulty capturing all vessels identified by the human labeler, all identified vessels are accurately labelled as perfused or not. This shows us the success of the 3D-CNN in the second step of the algorithm, and by extension, the 3D-CNN can predict if a vessel is flowing or not accurately. It is evident that the first step of the algorithm, the Steger Curvilinear vessel detector, results in most missed vessels not detected by the algorithm. Specifically, The Steger algorithm has difficulty in capturing 3 types of vessels, two vessels that are adjacent to each other, figure 5a, two vessels directly intersecting each other, figure 5b, or wide poorly outlined vessels (i.e., deep tissue vessels), figure 5c. Although the Steger algorithm is not as accurate as state-of-the-art machine-learning-based vessel segmentation schemes, it is robust enough to be applied to various imaging modalities and tissue types, unlike the machine-learning-based segmentation schemes which do not generalize very well to other applications.

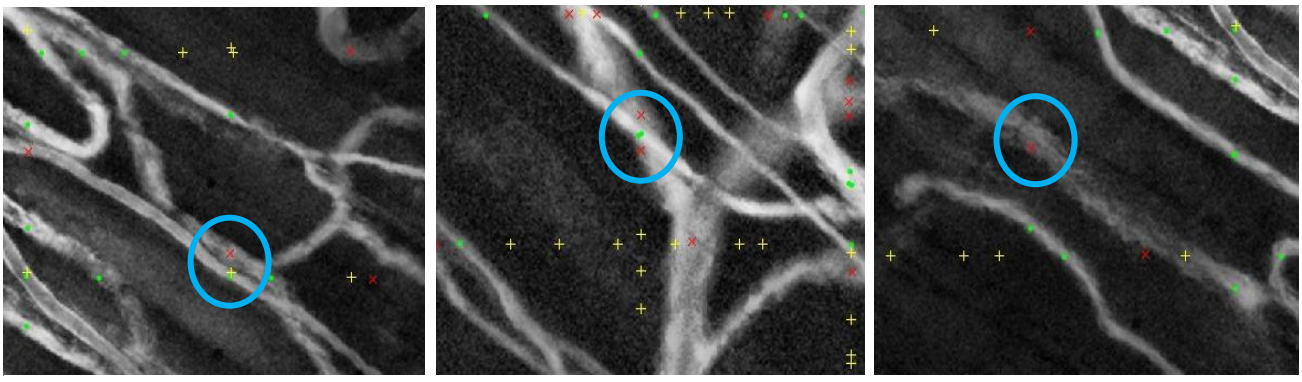

(a) (b) (c)

Figure 5. Example of three common missed vessel errors; resulting from the *Steger Curvilinear detector* (SCD), green dot is identified by both human labeller and SCD, yellow plus sign is found only by SCD, red "x" is found only by human and not by SCD. (a) two adjacent vessels seen as one vessel by SCD. (b) two vessels intersecting each other seen as one vessel by SCD. (c) poorly outlined vessel structure due to vessel depth prevents SCD from detecting vessel.

Conclusion and Future work

Functional analysis of microcirculation is a time consuming and mundane task that is more suited for a computer than a human to complete. The presented two-step algorithm for the functional analysis of the microcirculation allows the results of this study to act as a foundation for future work with functional microcirculation analysis. Achieving an accuracy of 90% compared to an expert allows this algorithm to be applied in a real-world setting.

Future work involves slight improvements in the algorithm pre- and post-processing steps. This can replace the Steger Curvilinear detector with a machine-learning-based algorithm trained on our local dataset, which will improve performance of the entire end-to-end algorithm

Acknowledgements

We would like to thank the researches, Irene Ying, Sanjana Arora, and Yanmin Zhang at the Centre for Critical Illness Research of the Lawson Health Research Institute for supplying and assisting in the labeling of the microcirculation videos.

References

Charlton, M.; Sims, M.; Coats, T.; Thompson, J. 2017. The microcirculation and its measurement in sepsis. *Journal of the Intensive Care Society*, 18(3):221–227. doi:10.1177/1751143716678638

Bezemer, R.; Dobbe, J.; Bartels, S.; Boerma, E.; Elbers, P.; Heger, M.; Ince, C. 2011. Rapid automatic assessment of microvascular density in sidestream dark field images. *Medical & Biological Eng. & Computing*, *49*(11):1269–1278. doi.org/10.1007/s11517-011-0824-1

De Backer, D.; Hollenberg, S.; Boerma, C.; Goedhart, P.; Büchele, G.; Ospina-Tascon, G.; Dobbe, I.; Ince, C.; 2007. How to evaluate the microcirculation: report of a round table conference. *Critical Care 11(5):*R101. doi.org/10.1186/cc6118

Demir, S.; Hakimzadeh, R.; Hargraves, R.; Ward, K.; Myer, E.; Najarian, K. 2012. An automated method for analysis of microcirculation videos for accurate assessment of tissue perfusion. *BMC Medical Imaging*, *12*(37):1–13. doi.org/10.1186/1471-2342-12-37

Demir, S.; Mirshahi, N.; Tiba M.; Draucker, G.; Ward, K.; Hobson R.; Najarian K. 2009. Image processing and machine learning for diagnostic analysis of microcirculation. *ICME Int. Conference on Complex Medical Engineering*, 1–5. doi.org/10.1109/ICCME.2009.4906669

Ellis C.; Jagger J.; Sharpe M. 2005. The microcirculation as a functional system. *Critical Care* 9(4). S3. doi.org/10.1186/cc3751

Japee, S.; Pittman, R.; Ellis, C. 2005. A New Video Image Analysis System to Study Red Blood Cell Dynamics and Oxygenation in Capillary Networks. *Microcirculation*, 12(6):489–506. doi.org/10.1080/10739680591003332

Jiang, Y.; Bainbridge-Smith, A.; Morris, A. 2007. Blood vessel tracking in retinal images. *Proceedings of Image and Vision Computing*, 126–131.

Lawendy, A-R; Bihari, A.; Sanders, D.; Badhwar, A.; Cepinskas, G. 2016. Compartment syndrome causes systemic inflammation in a rat. Bone Joint J. 98-B(8):1132–7. doi.org/10.1302/0301-620X.98B8.36325

Liu, C.; Gomez, H.; Narasimhan, S.; Dubrawski, A.; Pinsky, M.; Zuckerbraun, B. 2015. Real-time visual analysis of microvascular blood flow for critical care, *IEEE Conference on Computer Vision and Pattern Recognition* 2217-2225. doi.org/10.1109/CVPR.2015.7298834

Steger, C. 1998. An Unbiased Detector of Curvilinear Structures. *IEEE Trans. On Pattern Analysis And Machine Intelligence*. 20(2):113–125. doi.org/10.1109/34.659930

Tafner, P.; Chen, F.; Filho, R.; Corrêa, T.; Chaves, R.; Neto, A. 2017. Recent advances in bedside microcirculation assessment in critically ill patients. *Revista Brasileira de Terapia Intensiva*, *29*(2):238–247. doi.org/10.5935/0103-507X.20170033

Yeh, Y.; Chao, A.; Lee, C-Y.; Lee, C-T.; Yeh, C-C.; Liu, C-M; Tsai, M-K. 2017. An observational study of microcirculation in dialysis patients and kidney transplant recipients. European Journal of Clinical Investigation. *John Wiley & Sons, Ltd*. 47(9):630–637. doi.org/10.1111/eci.12784